Environment Protection Engineering

Vol. 49 2023 No. 2

DOI: 10.37190/epe230204

FATMA A-M. KASSEM (ORCID: 0000-0001-6888-5544)[1]
AHMED FAROUK ABDELGAWAD (ORCID: 0000-0002–2480-8229)[2]
A. E. ABU EL-EZZ (ORCID: 0009-0005-6585-8416)[3]
MOFREH M. NASSIEF (ORCID: 0009-0003-0216-1561)[2]
MOHAMED ADEL (ORCID: 0009-0007-7108-4220)[2]

INFLUENCE OF VENTILATION TO LIMIT AIRBORNE INFECTION CONCENTRATION IN AN ISOLATION ROOM

Coronavirus (COVID-19) was detected at the end of 2019 and has since caused a worldwide pandemic. This virus is transferred airborne. In this study, an investigation was carried out of the ventilation strategies inside the isolation room based on exhaust air locations. To reduce the infection disease (COVID-19), due to the spreading of exhaled contaminants by humans in interior environments, five models for ventilation systems differing in the position of the outlet and inlet were used. This study aims to increase knowledge regarding the exhaled contaminant distribution under different environmental conditions (opening exhaust and negative pressure). The results showed a good agreement between the computational results and the experimental data. Tracer gas CO_2 was used to evaluate the air quality experimentally and computationally. The results showed that stable conditions are obtained inside the room at a negative pressure value above –1.5 Pa. The residence time of the infected airborne decreases when the pressure difference increases. The study revealed that the model with an air outlet opening installed behind the patient enabled avoiding the spread of infection in the room.

SYMBOLS AND ABBREVIATIONS

ACH – air change per hour, 1/h
C – concentration, ppm
C_m – experimental model concentration, ppm
C_s – simulation concentration, ppm
CFD – computational fluid dynamics
f – frequency, 1/s
v_{max} – maximum velocity, m/s

[1]Department of Volume and Fluid Flow Metrology Laboratory, National Institute of Standards, Giza, Egypt, corresponding author F. A.-M. Kassem, email address: fatma.abdelmordy@nis.sci.eg
[2]Department of Mechanical Power Engineering, Faculty of Engineering, Zagazig University, Egypt.
[3]Department of Force and Material Metrology Laboratory, National Institute of Standards, Giza, Egypt.

$Q1$ – median of the lower half of the data, ppm
$Q3$ – median of the upper half of the data, ppm
DV – displacement ventilation
LAF – laminar airflow
MV – mixed ventilation
POV – protective occupancy ventilation
PV – personalized ventilation
SARS – severe acute respiratory syndrome
TB – tuberculosis
TVOC – total volatile organic compounds
UFAD – under-floor air distribution
WAV – wall air ventilation

1. INTRODUCTION

The ventilation of the isolation room is important for controlling patients' exhaled contaminants' dispersion. Many infectious agents such as tuberculosis (TB) [1], severe acute respiratory syndrome (SARS) [2], and COVID-19 [3] are transferred by aerosols. The experience with COVID-19, from 2019 till now, has activated increased consideration of the problem of aerosol transmission. The small distance between healthcare workers and their patients increases the transmission of infection [3–5]. Exhaled transmission of contaminants may be controlled by the use of a negative-pressure isolation room [6]. However, when the door of an isolation room is opened, the condition inside the room fails to give the required negative pressure difference inside [7].

Various researchers proposed different ventilation forms such as displacement ventilation (DV), mixed ventilation (MV), wall air ventilation (WAV), underfloor air distribution (UFAD), protective occupancy ventilation (POV), personalized ventilation (PV), and laminar airflow (LAF). Two ventilation systems have been recommended for hospitals, which are DV and MV [8–10]. A new technique has been developed to overcome the shortage of airborne isolation rooms and to decrease healthcare worker exposure during a novel COVID-19. With the increase in the number of patients, hospitals have become crowded. Full rooms can become isolation rooms when negative pressure is created inside them [11–14]. This strategy has the benefit of using space and protecting other patients and healthcare workers outside the room [15]. One of the recommended ways to protect against the risk of infection is to wear masks such as N-95 masks [16, 17]. Table 1 explains the design parameters for isolation rooms to prevent airborne contamination for different organizations in multiple countries.

This study aimed to investigate the effect of the ventilation system position on reducing airborne transmission from the patient to the healthcare in a one-bed isolation room using both experimental and computational methods. Five models of exhaust air locations, with different positions inside the room, are shown in Table 2.

Table 1

Design standards for isolation rooms to prevent airborne contamination [18]

Country	Organization	ACH	Negative pressure inside the room [Pa]
UK	Department of Health	>10	>5.0
USA	Center for Disease Control and Prevention	>6	>2.5
Korea	Centers for Disease Control and Prevention	>6	>2.5
Australia	Department of Health and Human Services	>12	>5.0
Canada	Public Health Agency of Canada	>6	–
Norway	Norwegian Institute of Public Health	>12	>5.0
Hong Kong	Infection Control Committee Department of Health	>6	>2.5

Table 2

Study models

Model	Description of location	
	Air supply	Air outlet
1	the wall near the ceiling	the opposite wall behind the patient, above the floor by 0.95 m
2		the side wall to the right of the patient, above the floor by 0.82 m
3		the opposite wall the behind patient, above the floor by 0.05 m
4		the same wall in front of the patient above the floor by 0.05 m
5		inside the wall to the left of the patient above the floor by 0.25 m

2. MATERIALS AND METHODS

Details of the experiments. Experiments were carried out in a full-scale chamber with dimensions 2×2×2 m with different air-exhaust locations as shown in Fig. 1. The walls of the room were well insulated such that during the experimental measurements the mean room air temperature was kept constant within the range 21±2 °C. Five different air-distribution-outlet strategies were tested with the same inlet location and different outlet locations for models 1–5.

For all strategies, the inlet opening dimension was 0.60×0.20 m, and the outlet 0.35×0.35 m. The isolation room was illuminated with 18 W/m^2. The study had a patient lying on a bed at a height of 0.7 m from the floor. Each experiment was carried out with only one diffuser and one exhaust opening. Thermal breathing two manikins (the patient and the healthcare worker) and one lamp were placed in the room. During the experiments, the ventilation system supplied air at 22 °C, and the air change per hour (ACH) of 27 was defined according to Eq. (1) [19]:

$$\mathrm{ACH} = \frac{\text{Volume flow rate at the inlet}}{\text{room volume}} \tag{1}$$

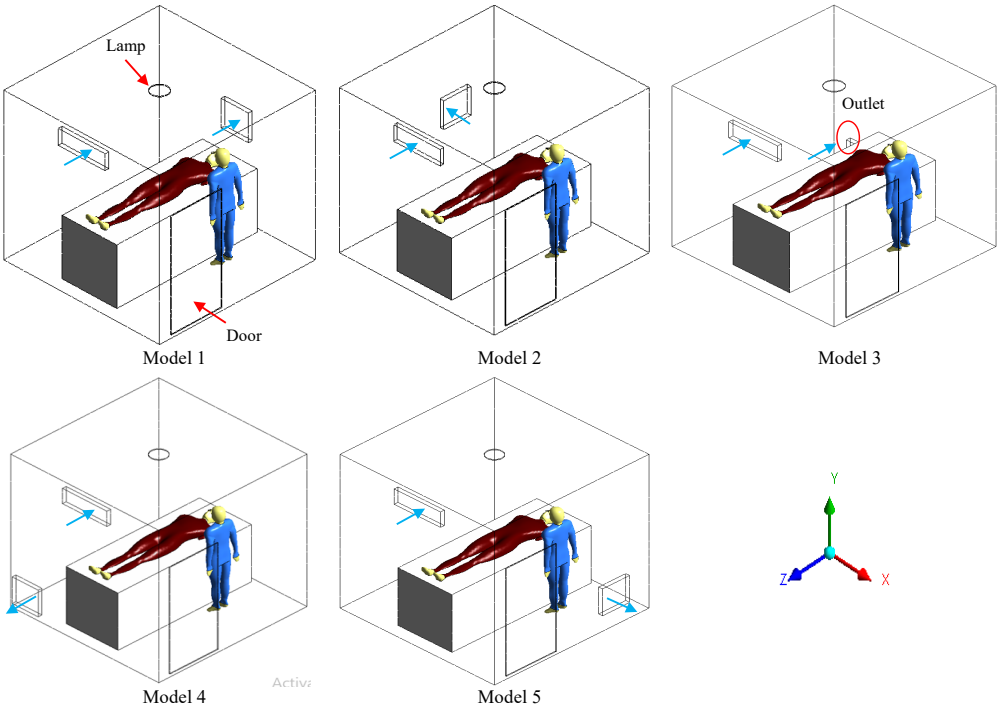

Fig. 1. Arrangements of the study models

a) location of measuring points b) nose and injection source c) data acquisition system

Fig. 2. Measuring points

To achieve stable conditions, the room was allowed to stabilize for an hour before taking measurements. In the experiments, both manikins exhaled through the nose. The nostrils formed an angle with a horizontal plane of about 30°. The nose consisted of two holes, each of which was 5 mm in diameter. The respiratory minute volume was 9 dm^3/min and the breathing frequency was 15 min^{-1} [19, 20]. Tracer gas CO_2 was injected from the patient nose. The injection rate of CO_2 was regulated via a rotameter and continuously released from a cylinder as a point emitting tracer gas at 0.60 dm^3/exhaled stock (15 min^{-1}) as seen in Fig. 2b. The injection was controlled using a solenoid valve-connected timer (Fig. 2c). The concentration of tracer gas was measured continuously using an air quality sensor from 400 to 29 206 ppm at five locations. Three sampling points (P1, P2, and P3) were installed inside the room to evaluate the concentration of CO_2. Also, the total volatile organic compound (TVOC) was measured using air quality sensors from 0 to 32 768 ppm, which were located around the bed at 1.0 m from the floor to monitor the exposure level of the healthcare staff at these locations by the computerized system using an interface between Arduino and lab-view software as shown in Fig. 2c. One sampling point (P4) was installed at the exhaust grille to evaluate the amount of CO_2 removed from the room as shown in Fig. 2a, and the P5 sensor was installed in a corridor behind the door to monitor the leakage from the room while the door was closed. The negative pressure was created inside the isolation room using a blower (with a capacity of 12 000 m^3/h and power of 2.6 kW).

Computational fluid dynamics (CFD) setup. The CFD simulation was done utilizing the Fluent package of ANSYS 2016 [21]. According to this package, the governing equations in three-dimensional form, the continuity equation, and momentum equations using *K-ε* RNG turbulence were solved [5] with transient analysis. The unstructured mesh of the model was generated using approximately 1.92×10^6 elements as shown in Fig. 3a.

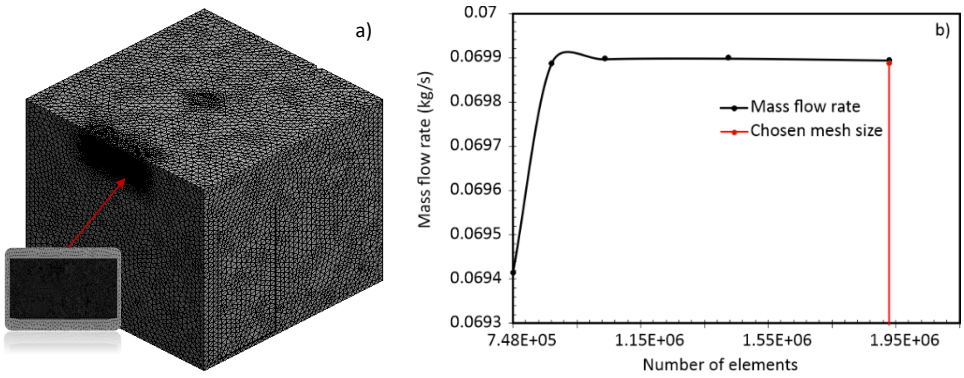

Fig. 3. Mesh configuration (a) and sensitivity (b)

Table 3

Properties of the mesh

Property	Value
Element minimum size, mm	0.1
Element maximum size, mm	0.2
Growth rate, dimensionless	1.2
Curvature normal angle, deg	18
Inflation transition ratio	0.272
Inflation number of layers	5
Number of elements	1 925 737

Table 4

CFD models and boundary conditions

Model	Item	Description
Viscous model	K-ε	RNG
	near wall treatment	standard wall function
Energy	on	
Species	Species transport	CO_2, H_2O
Discrete phase	on	
	particle treatment	unsteady particle tracking
	material injection	water
	injection type	surface
	particle type injection	water liquid
Boundary conditions		
Inlet	velocity	0.5 m/s
	temperature	295 K
	discrete phase BC type	escape
Inlet mouth	velocity	
	velocity component	UDF (user-defined function)
	V_x	0
	V_y	$1.99t\sin(\pi/2)\sin(\pi/6)$
	V_z	$1.99t\sin(\pi/2)\cos(\pi/6)$
	temperature	300 K
	CO_2 mole fraction	0.3%
	H_2O mole fraction	0.2%
	discrete phase BC type	escape
Outlet	gauge pressure	0
	discrete phase BC type	escape
Walls	wall motion	stationary wall
	heat flux	0
	species	zero diffusivity flux
	discrete phase BC type	reflect
Lamp	heat flux	18 W/m^2

The properties of the mesh are shown in Table 3. The fluid domain was defined as air at 25 °C from the ANSYS models library. The solid domains of the model were defined as no-slip walls. The breathing function was a very important point in the simulation. The manikin breathes following a sinusoidal function according to the equation:

$$v = 1.99 \sin \frac{\pi}{2} t \tag{2}$$

where the maximum velocity v_{max} = 1.99 m/s and frequency f = 0.25 s^{-1}.

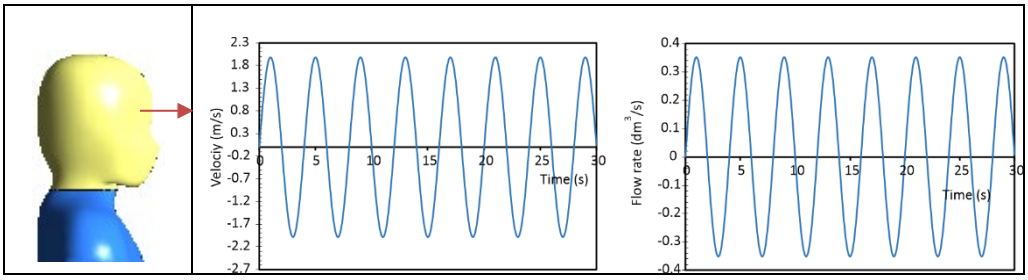

Fig. 4. Breathing function

During a half period, the manikin was exhaling, and during the other half it was inhaling (Fig. 4). The volume flow rate was 0.60 dm^3/exhalation at 27 °C. Boundary conditions are given in Table 4.

3. RESULTS AND DISCUSSION

3.1. VALIDATION AND PREDICTION OF THE NUMERICAL MODEL

The mean CO_2 concentrations for the experimental results and CFD simulation for model 1 are listed in Table 5. There is a good agreement between experimental and computational results. The percentage of the variance between the simulation and measurement results varies from –11.57 to 3.18%. The average reference value of CO_2 inside the room before CO_2 injection, taken during the measurement, is 410 ppm. The tracer gas was used to calculate how concentrations of CO_2 were diminished.

Table 5

Simulation and experimental CO_2 concentrations for model 1 [ppm]

Sample point	CFD simulation C_s	Measurement C_m	$\frac{C_s - C_m}{C_m} \times 100\%$
P1	8.25	9.14	–9.78
P2	4.51	5.10	–11.57
P3	6.16	5.97	3.18

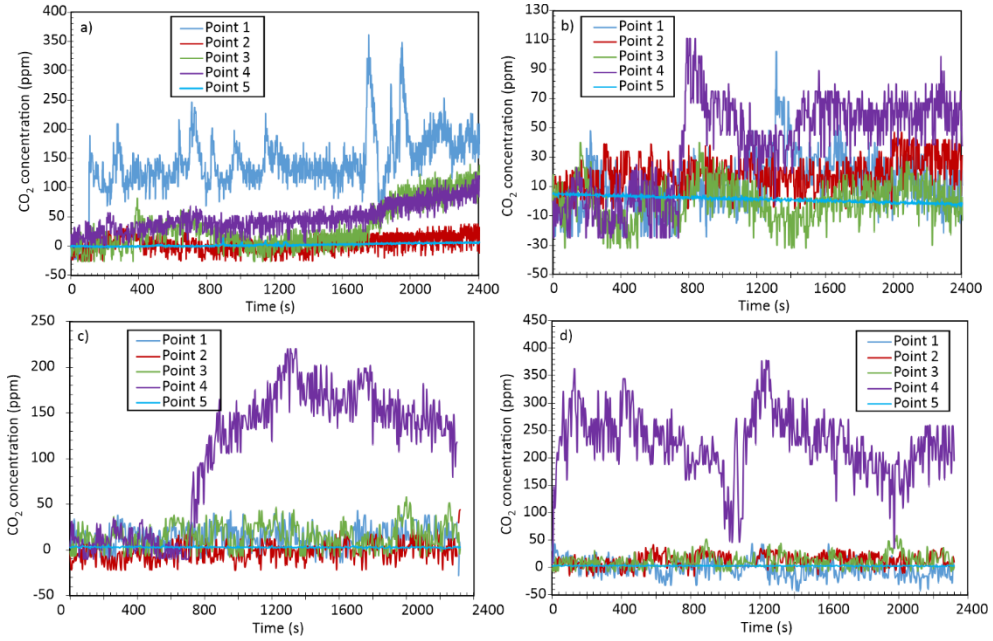

Fig. 5. CO_2 concentrations with various negative pressures (Pa) inside the room for model 1: a) 0, b) –0.5, c) –1.5, d) –2.5

Figure 5 shows the time dependences of CO_2 concentration in the indoor environment for model 1. Air did not mix or diffuse inside the room, but it was quickly sucked through exhaust grilles placed behind the patient's head. This is due to the negative pressure created. As CO_2 was injected, the tracer gas concentration increased rapidly at the monitoring locations P1–P4, while the concentration of CO_2 in P5 was roughly zero. This indicates that there was no leakage from the room to the surrounding environment when the door was closed. On the contrary, when the pressure difference equaled zero, the air of the indoor environment mixed and spread into the room. This causes an increased concentration at the three sampling measuring points (P1, P2, and P3) located around the patient as shown in Fig. 5a. The CO_2 concentration inside the room decreased with the pressure difference increase, for example, the time for the CO_2 pollutant to reach the outlet inside the isolation chamber for a pressure difference of –1.5 Pa is equal to 10 minutes, as shown in Fig. 5c. While for –2.5 Pa, it was approximately 2 minutes as shown in Fig. 5d. In addition, the CO_2 concentration profiles for the P1 and P2 sampling points when negative pressure is established are approximately similar, and this is evidence to reach stable environmental conditions. At P4, the measuring point at the exhaust grille, the CO_2 concentration continued to maintain a higher value than the other three monitoring locations over the period of measurement. The average concentration of CO_2 on P4 was 50–300 ppm for the case –2.5 Pa. These represent ten times higher gas concentration than that for P1, in which the concentration was up to 10 ppm, P2 up to 5 ppm, and P3 up to 10 ppm.

3.2. VOLATILE ORGANIC COMPOUNDS (VOCs)

The concentration of VOCs depends on the concentration of CO_2, due to the existence of the compound oxygen and carbon. The reference value of VOCs during the measurement was 1 ppm. The profile trend of VOCs concentration was similar to the trend of the CO_2 concentration profile as shown in Fig. 6.

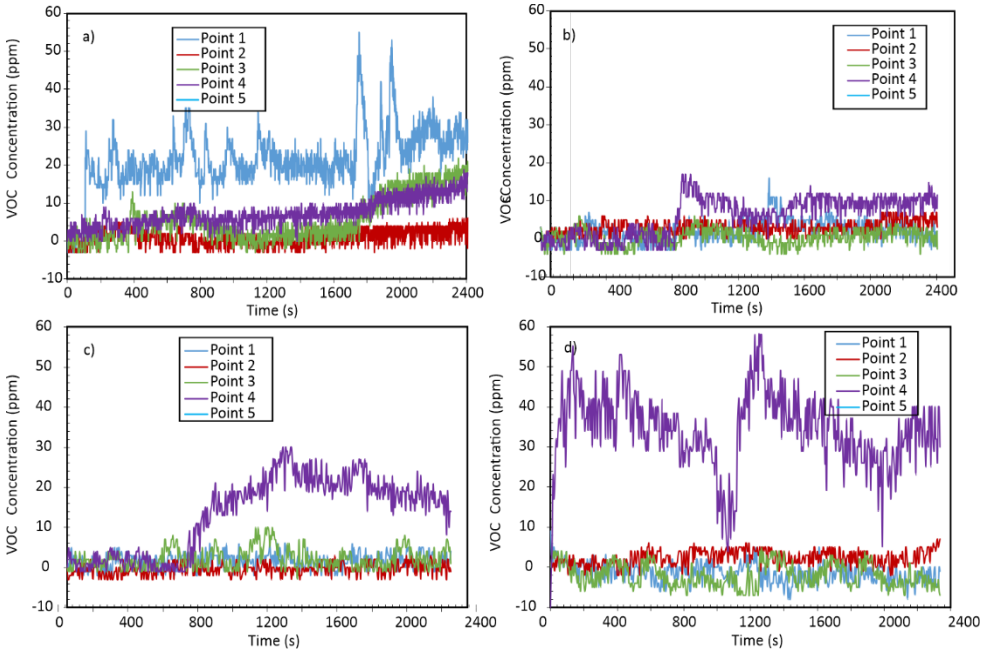

Fig. 6. VOCs concentrations with various negative pressures (Pa) inside the room for model 1: a) 0, b) –0.5, c) –1.5, d) –2.5

The results confirmed that as the concentration of CO_2 increased, the concentration of VOCs increased as well. The measured concentration of VOCs around the patient on the bed was about 2 ppm. This recommended value of VOCs concentration is less than 3 ppm [22–24].

The measured concentration of CO_2 at different sampling points (P1, P2, P3) as shown in Fig. 7 is approximately similar with a little deviation of 6 ppm (Q1–Q3) during the experiments for most models, for example, model 1. This model is reasonably accurate to estimate the concentration profile of airborne contaminants in the isolation room. The simulation showed good agreement with the results of measurement. The simulation technique was used to perform additional analysis when the experimental technique was not applicable. The simulation work was used to the multi-component gas type and emission rate of the source CO_2 according to Eq. (2).

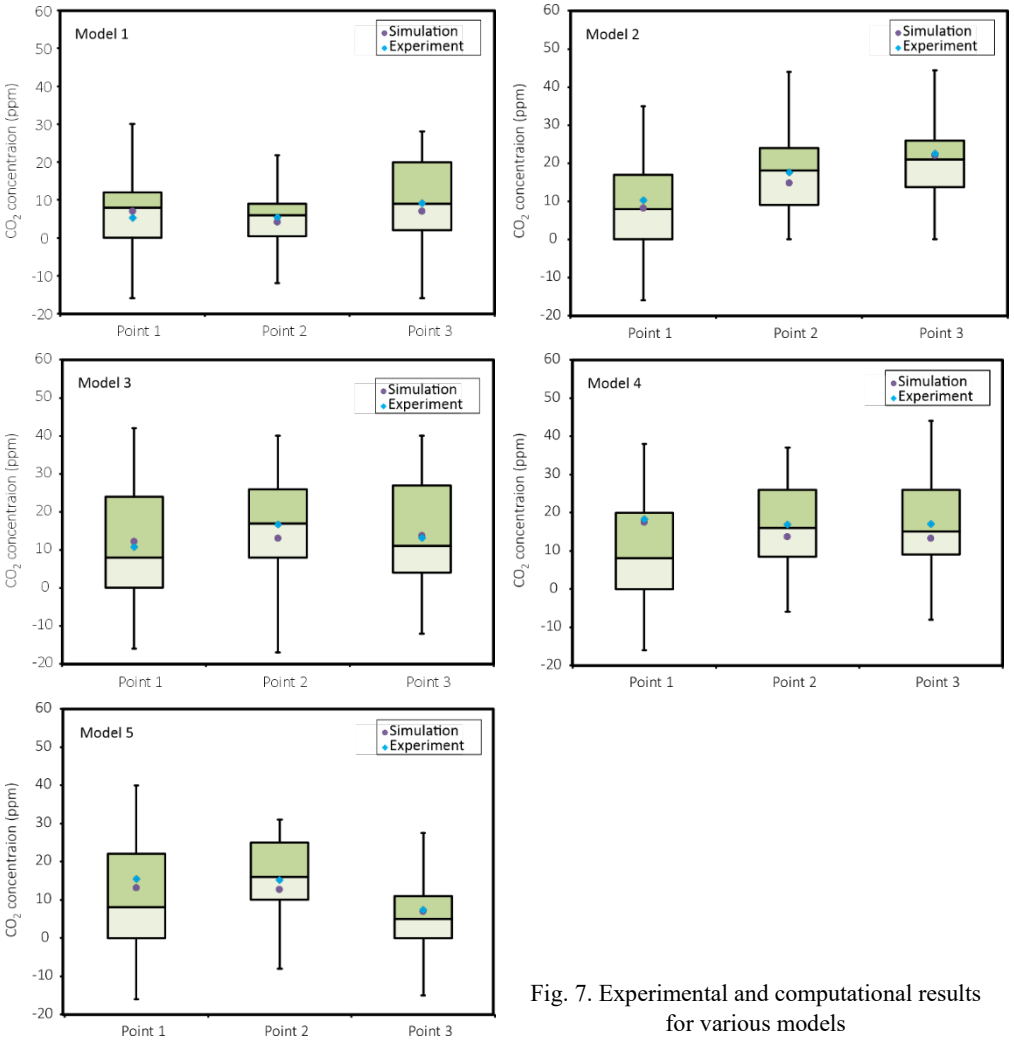

Fig. 7. Experimental and computational results for various models

3.3. VENTILATION EFFECTIVENESS

The average concentration level of airborne pollutants emitted from the patient inside the isolation room for different models with difference pressure –2.5 Pa is shown in Fig. 8.

Ventilation with model 4 gave a high concentration of CO_2, which ranged between 16.9 and 18 ppm. The lowest CO_2 concentration was detected for model 1, which ranged between 5.15 and 9.11 ppm. The CO_2 concentration range between 10.28 and 22.47 ppm was detected for model 2.

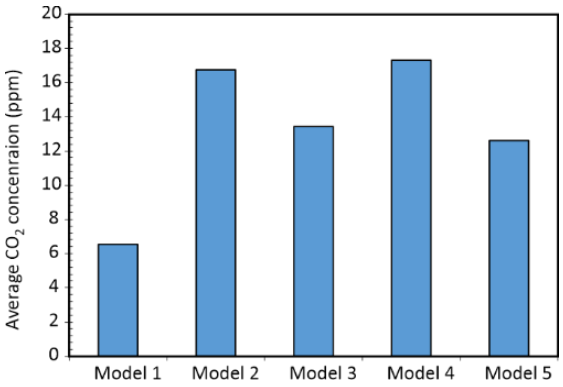

Fig. 8. Average CO_2 concentrations inside the isolation room at –2.5 Pa for various models

1 m above the floor around the bed, the average CO_2 airborne concentration, for example, for model 5 was 24.93% lower than for model 2. Similarly, model 1 was more effective in removing contaminants in the room. For this model, the average CO_2 concentration was 2-fold lower than for model 3 and nearly 3-fold lower than for models 2 and 4. The obtained results indicate that the installation of the exhaust opening behind the patient is better than the installation at the left and right sides of the patient bed.

3.4. WATER–LIQUID RESIDENCE TIME

Figure 9 shows the water–liquid particle time-residence inside the room with a mole fraction of 0.02 and a diameter range from 0.5 to 1 μm [20, 25]. For a pressure difference of 0 Pa, the time residence of water–liquid inside the room reached 214.5 s. The time-residence decreased with a pressure difference of –1.5 Pa to 47 s for model 2, and similarly for other models. This proves that with increased pressure difference, the time-residence of water-liquid particles, carriers of infection, decreased.

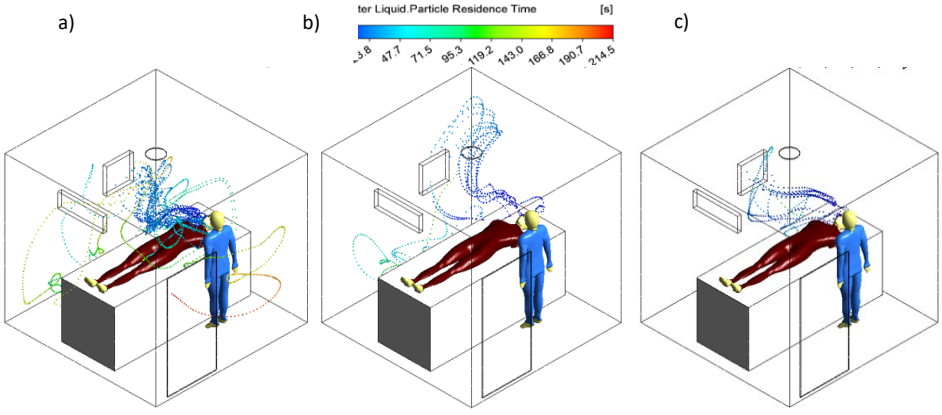

Fig. 9. Water-liquid particle time residence for model 2 at various pressure differences (Pa): a) 0, b) –0.5, c) –1.5

3.5. DISTRIBUTION OF THE CO_2 CONCENTRATION, RELATIVE HUMIDITY, AND AIR VELOCITY IN THE ROOM

The concentration distribution patterns for different models are shown in Fig. 10 at a 1 m horizontal plane, representing the respiration level of the healthcare workers during treating the patient.

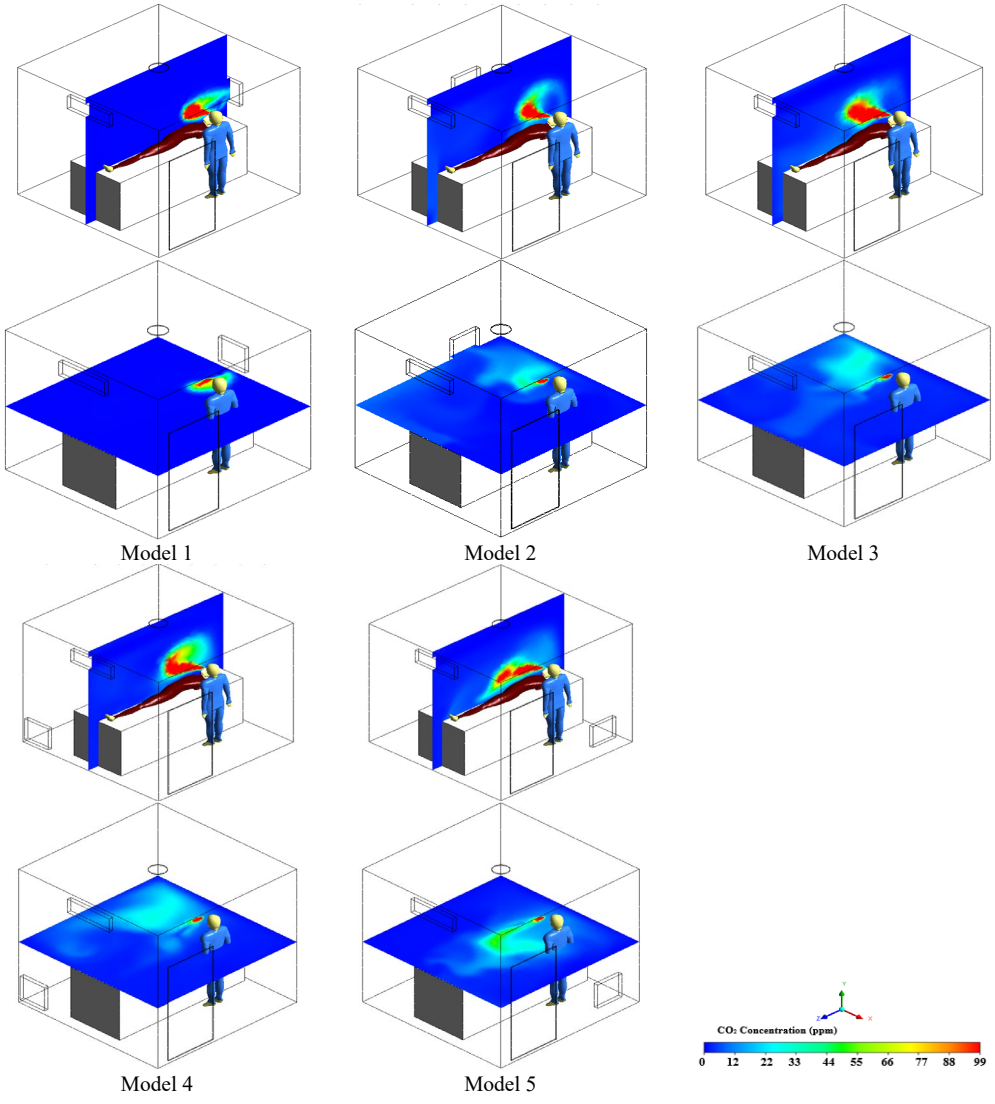

Fig. 10. CO_2 concentration contours for various models after 214 s under a pressure difference of –2.5 Pa

The high concentration of CO_2 in front of the patient decreased as they moved away from the patient. The small regions of high concentration for model 1, compared with other models, are due to the small distance between the source of the pollutant (nose) and the exhaust location. On the contrary, model 4, due to increasing the distance between the source and the exhaust location, lead to an increase of pollutant regions until exit from the exhaust opening. In this research, the location of the exhaust opening is very important for removing airborne pollutants from the patient.

Figure 11 shows the deviation of relative humidity (the average reference relative humidity taken during the measurement is 42%) with different pressure values inside the room. It was found that relative humidity profiles at the two monitoring points (P1 and P3) in the isolation room increased with time. It was observed that the relative humidity profile has not reached stability, and more time is needed to reach equilibrium inside the room for the pressure difference to equal zero. However, when negative pressure was created in the room, equilibrium of environmental conditions can be reached after 2 min. Also, it was found that there was a similar profile for all cases. This shows evidence of the stability and accuracy of the measuring sensor and the suitability of the boundary conditions in this study.

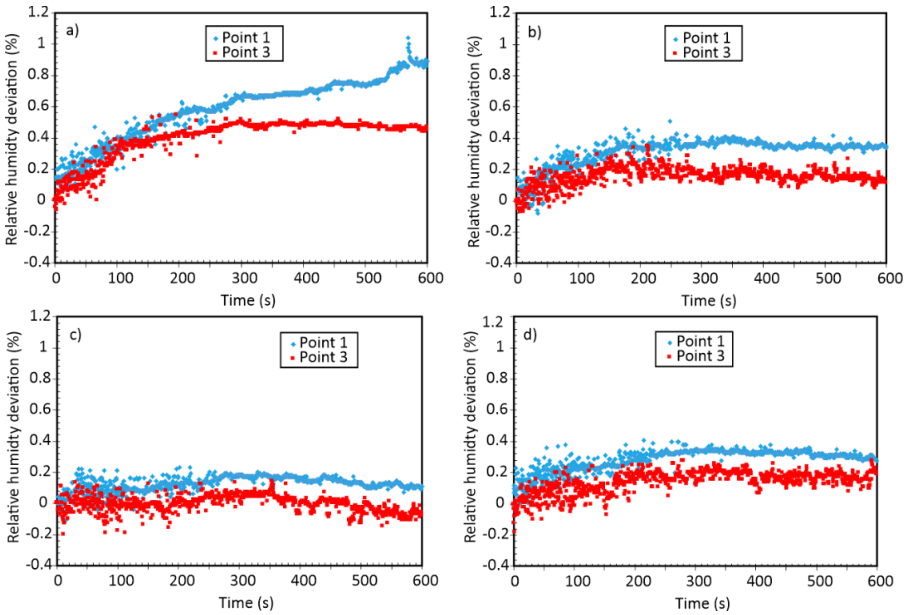

Fig. 11. Relative humidity deviations with various pressure differences inside the room for model 1 (Pa): a) 0, b) –1.0, c) –1.5, d) –2.5

The velocity distributions around the patient at different pressures inside the room are shown in Fig. 12. The airflow towards the patient was discharged via one exhaust grille mounted on the wall behind the patient in the room. The patient on the bed was

experiencing about 0.10 m/s airflow. The recommended value of air velocity is less than 0.25 m/s [22–24]. It is concluded that the negative pressure does not affect the velocity profile at the pressure above –1.5 Pa. This means that the stability of indoor environmental conditions is suitable at –1.5 Pa.

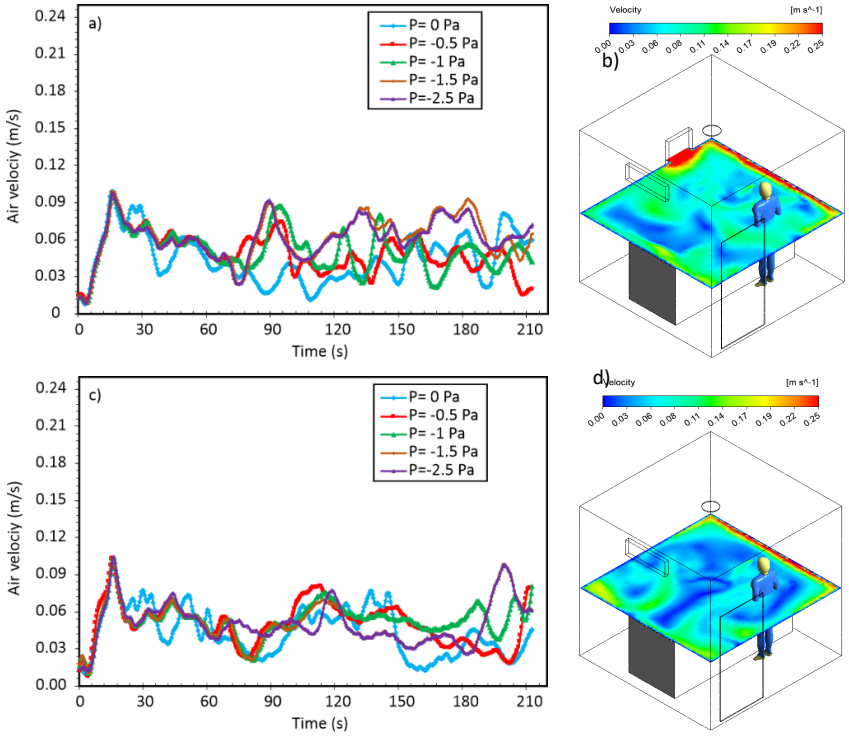

Fig. 12. Air velocity contours inside the room: contour (a) corresponding to model 2 (b) and contour (c) corresponding to model 3 (d)

4. CONCLUSIONS

- Locations of the inlet and exhaust openings are the most important elements that directly affect the pollutants dispersion in the room.
- The distance between the patient and the exhaust location is very important to reduce the regions of pollutants when the air flows move towards the exhaust opening, due to the reaction of dynamic forces.
- At 1 m above the floor around the patient bed, the average pollutant concentration for model 5 was 27.27% lower than that for model 4.

• Model 1 was more effective for removing pollutants in the isolation room than models 2–5. For model 1, the mean CO_2 concentration was lower by 61.12, 51.52, 62.33, and 48.21% than for models 2, 3, 4, and 5, respectively;

• To get possible constant conditions around the patient and reach equilibrium inside the room in a short time, the pressure difference value must be above –1.5 Pa;

• The boundary conditions are appropriate because the air velocity around the patient did not exceed 0.25 m/s.

• Good agreement between the experimental and simulation results was achieved. This is the evidence for the compatibility of the boundary conditions used in the simulation.

It is recommended that, due to the highest concentration of the infection gas, healthcare workers should not stand near the outlet opening of isolation rooms containing patients. For the location of the outlet opening, it is recommended to be installed behind the patient to avoid the spread of infection in the room.

REFERENCES

[1] FENNELLY K.P., MARTYNY J.W., FULTON K.E., ORME I.M., CAVE D.M., HEIFETS L.B., *Cough-generated aerosols of Mycobacterium tuberculosis: a new method to study infectiousness*, Am. J. Respir. Crit. Care Med., 2004, 169 (5), 604–609. DOI: 10.1164/rccm.200308-1101OC.

[2] YU I.T.S., LI Y., WONG T.W., TAM W., CHAN A.T., LEE J.H.W., LEUNG D.Y.C., HO T., *Evidence of airborne transmission of the severe acute respiratory syndrome virus*, N. Eng. J. Med., 2004, 350 (17), 1731–1739. DOI: 10.1056/NEJMoa032867.

[3] RENDANA M., *Impact of the wind conditions on COVID-19 pandemic. A new insight for direction of the spread of the virus*, Urban Clim., 2020, 34, 100680. DOI: 10.1016/j.uclim.2020.100680.

[4] LI Y., HUANG X., YU I.T., WONG T.W., QIAN H., *Role of air distribution in SARS transmission during the largest nosocomial outbreak in Hong Kong*, Indoor Air, 2005, 15 (2), 83–95. DOI: 10.1111/j.1600-0668.2004.00317.

[5] ZHANG Z., CHEN Q., *Experimental measurements and numerical simulations of particle transport and distribution in ventilated rooms*, Atmos. Environ., 2006, 40 (18), 3396–3408. DOI: 10.1016 /j.atmosenv.2006.01.014.

[6] SARAVIA S.A., RAYNOR P.C., STREIFEL A.J., *A performance assessment of airborne infection isolation rooms*, Am. J. Infect. Control, 2007, 35 (5), 324–331. DOI: 10.1016/j.ajic.2006.10.012.

[7] KALLIOMÄKI P., HAGSTRÖM K., ITKONEN H., GRÖNVALL I., KOSKELA H., *Effectiveness of directional airflow in reducing containment failures in hospital isolation rooms generated by door opening*, Build. Environ., 2019, 158, 83–89. DOI: 10.1016/j.buildenv.2019.04.034.

[8] YANG B., MELIKOV A.K., KABANSHI A., ZHANG C., BAUMAN F.S., CAO G., LIN Z., *A review of advanced air distribution methods-theory, practice, limitations and solutions*, Energy Build., 2019, 202, 109359. DOI: 10.1016/j.enbuild.2019.109359.

[9] MELIKOV A.K., *Advanced air distribution: improving health and comfort while reducing energy use*, Indoor Air, 2016, 26 (1), 112–124. DOI: 10.1111/ina.12206.

[10] CAO G., AWBI H., YAO R., FAN Y., SIRÉN K., KOSONEN R., ZHANG J.J., *A review of the performance of different ventilation and airflow distribution systems in buildings*, Build. Environ., 2014, 73, 171–186. DOI: 10.1016/j.buildenv.2013.12.009.

[11] BRUNEKREEF B., FORSBERG B., *Epidemiological evidence of effects of coarse airborne particles on health*, Eur. Respir. J., 2005, 26 (2), 309–318. DOI: 10.1183/09031936.05.00001805.
[12] DYER J., *COVID-19 forced hospitals to build negative pressure rooms fast*, Infect. Control Today, 2020.
[13] MOUSAVI E.S., POLLITT K.J.G., SHERMAN J., MARTINELLO R.A., *Performance analysis of portable HEPA filters and temporary plastic anterooms on the spread of surrogate coronavirus*, Build. Environ., 2020, 183, 107186. DOI: 10.1016/j.buildenv.2020.107186.
[14] MOUSAVI E.S., NAFCHI A.M., DESJARDINS J.D., LEMATTY A.S., FALCONER R.J., ASHLEY N.D., MOSCHELLA P., *Design and in-vitro testing of a portable patient isolation chamber for bedside aerosol containment and filtration*, Build. Environ., 2020, 207, 108467. DOI: 10.1016/j.buildenv.2021. 108467.
[15] DAO H.T., KIM K.S., *Behavior of cough droplets emitted from COVID-19 patient in hospital isolation room with different ventilation configurations*, 2022, Build. Environ., 209, 108649. DOI: 10.1016 /j.buildenv.2021.108649.
[16] SARKIS-ONOFRE R., DO CARMO BORGES R., DEMARCO G., DOTTO L., SCHWENDICKE F., DEMARCO F.F., *Decontamination of N95 respirators against SARS-CoV-2. A scoping review*, J. Dent., 2021, 104, 10353. DOI: 10.1016/j.jdent.2020.103534.
[17] GRINSHPUN S.A., YERMAKOV M., *Impact of face covering on aerosol transport patterns during coughing and sneezing*, J. Aerosol Sci., 2021, 158, 10584. DOI:. 10.1016/j.jaerosci.2021.105847.
[18] CHO J., *Investigation on the contaminant distribution with improved ventilation system in hospital isolation rooms: Effect of supply and exhaust air diffuser configurations*, Appl. Therm. Eng., 2019, 148, 208–218. DOI: 10.1016/j.applthermaleng.2018.11.023.
[19] KASSEM F.A., ABDELGAWAD A.F., ABUEL-EZZ A.E., NASSIEF M.M., ADEL M., *Design and performance evaluation of a portable chamber for prevention of aerosol airborne infection*, J. Adv. Res. Fluid Mech. Therm. Sci., 2022, 100 (2), 181–197. DOI: 10.37934/arfmts.100.2.181197.
[20] KASSEM F.A., ABDELGAWAD A.F., ABUEL-EZZ A.E., NASSIEF M.M., SAMAHA S.H., ADEL M., *Performance evaluation of different texture material masks to reduce airborne infection*, CFD Lett., 2023, 15 (7).
[21] FLUENT. *Fluent 16.0 User's Guide.*
[22] KASSEM F.A., ABDELGAWAD A.F., ABUEL-EZZ A.E., NASSIEF M.M., ADEL M., *Recent preventive methods to reduce the infection diseases by air distributions control*, J. Measure. Sci. Appl., 2023, 1 (1). DOI: 10.21608/JMSA.2023.288124.
[23] ASHRAE 62.1.2009, *Calculation of CO_2 concentration in a zone*, Retrieved Sep. 23th, 2016.
[24] *Guidelines for Indoor Air Quality*, King Mongkut's University of Technology Thonburi, 2013.
[25] LIU Y., NING Z., CHEN Y., GUO M., LIU Y., GALI N.K., DUAN Y., CAI J., WESTERDAHL D., LIU X., XU K., HO K.F., KAN H., FU Q., LAN K., *Aerodynamic analysis of SARS-CoV-2 in two Wuhan hospitals*, Nature, 2020, 582 (7813), 557–560. DOI: 10.1038/s41586-020–2271-3.